JBMR Plus, 2025, **9**, ziae142
https://doi.org/10.1093/jbmrpl/ziae142
Advance access publication: November 9, 2024
Research Article

Lysine specific demethylase 1 conditional myeloid cell knockout mice have decreased osteoclast differentiation due to increased IFN-β gene expression

Kristina Astleford-Hopper[1], Juan E. Abrahante Llorens[2], Elizabeth W. Bradley[3,*], Kim C. Mansky[4,*]

[1]Oral Biology Graduate Program, University of Minnesota School of Dentistry, Minneapolis, MN 55455, United States
[2]Minnesota Supercomputing Institute, University of Minnesota, Minneapolis, MN 55455, United States
[3]Department of Orthopedic Surgery and Stem Cell Institute, University of Minnesota, Minneapolis MN 55455, United States
[4]Division of Orthodontics, Department of Developmental and Surgical Sciences, University of Minnesota School of Dentistry, Minneapolis, MN 55455, United States
*Corresponding authors: Elizabeth W. Bradley, 2001 6th Street SE, Department of Orthopedic Surgery and Stem Cell Institute, University of Minnesota, Minneapolis, MN 55455, United States (Ebradle1@umn.edu) and Kim C. Mansky, 16-146 Moos Tower, 515 Delaware St SE, Department of Developmental and Surgical Science, University of Minnesota, Minneapolis MN 55455, United States (Kmansky@umn.edu)

Abstract

Osteoclasts are large multinucleated cells that degrade bone mineral and extracellular matrix. Investigating the epigenetic mechanisms orchestrating osteoclast differentiation is key to our understanding of the pathogenesis of skeletal related diseases such as periodontitis and osteoporosis. Lysine specific demethylase 1 (LSD1/KDM1A) is a member of the histone demethylase family that mediates the removal of mono- and dimethyl groups from H3K4 and H3K9 to elicit dichotomous effects on gene expression. Prior to our study, little was known about the contributions of LSD1 to skeletal development and osteoclast differentiation. Here we show that conditional deletion of *Lsd1* within the myeloid lineage or macrophage/osteoclast precursors results in enhanced bone mass of male and female mice accompanied by diminished osteoclast size in vivo. Furthermore, *Lsd1* deletion decreased osteoclast differentiation and activity within in vitro assays. Our bulk RNA-SEQ data suggest *Lsd1* ablation in male and female mice inhibits osteoclast differentiation due to enhanced expression of interferon-β target genes. Lastly, we demonstrate that LSD1 forms an immune complex with HDAC1 and HDAC2. These data suggest that the combination of methylation and acetylation of histone residues, facilitated by LSD1, mechanistically promotes osteoclast gene expression.

Keywords: osteoclasts, epigenetics, genetic animal models, cell/tissue signaling, transcription factors

Lay Summary

Osteoclasts are cells found in the bone that are responsible for bone resorption. Understanding mechanisms that regulate osteoclasts are critical as osteoclasts become more active in postmenopausal women potentially leading to bone loss. One mechanism to regulate osteoclast differentiation and activity are proteins that regulate DNA accessibility. We demonstrate that loss of one of these proteins that regulate DNA accessibility, lysine specific demethylase 1 (LSD1), results in smaller osteoclasts and a thicker skeletal phenotype in a mouse model. We demonstrate that loss of LSD1 expression in osteoclasts increases expression of interferon-β target genes, which are negative regulators of osteoclast differentiation. Collectively our data suggest that LSD1 is a positive regulator of osteoclast differentiation by down regulating the expression of negative regulators of osteoclast differentiation.

Received: October 15, 2024. **Revised:** October 25, 2024. **Accepted:** November 5, 2024
© The Author(s) 2024. Published by Oxford University Press on behalf of the American Society for Bone and Mineral Research.
This is an Open Access article distributed under the terms of the Creative Commons Attribution Non-Commercial License (https://creativecommons.org/licenses/by-nc/4.0/), which permits non-commercial re-use, distribution, and reproduction in any medium, provided the original work is properly cited. For commercial re-use, please contact journals.permissions@oup.com

Graphical Abstract

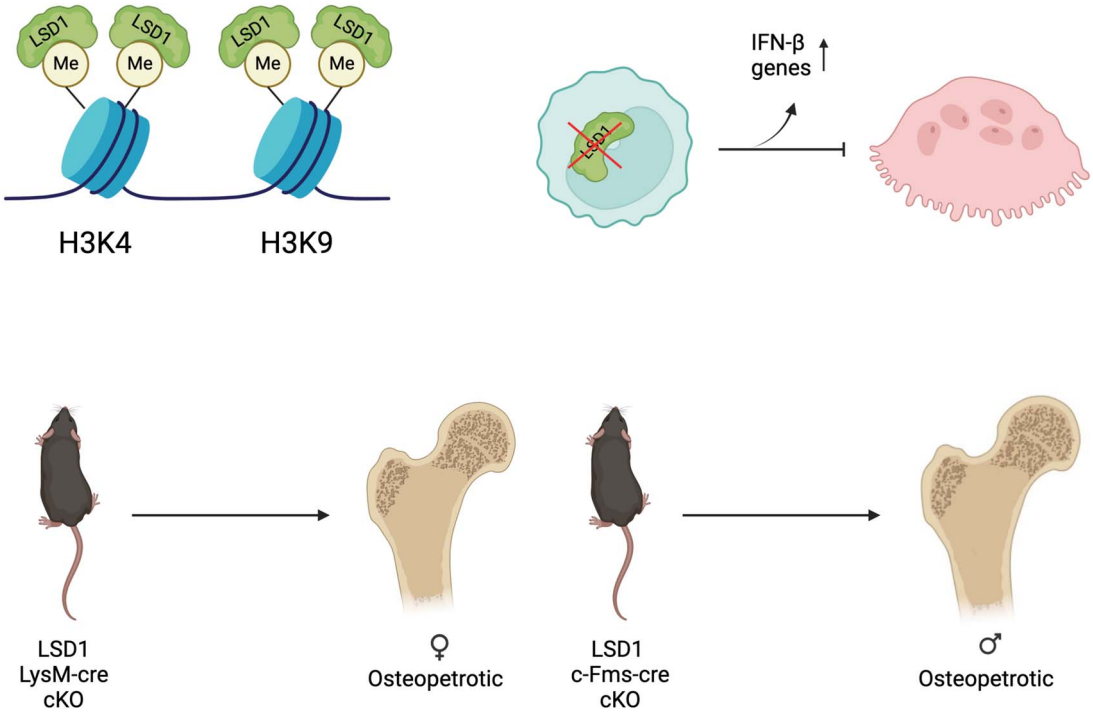

Introduction

Osteoclasts are large multinucleated cells responsible for resorbing bone mineral and extracellular matrix by secretion of catalytic enzymes and acids such as tartrate-resistant acid phosphatase (TRAP) and cathepsin K.[1] Osteoclasts play an important role in the bone remodeling process by breaking down worn out or broken bone. Osteoclasts also subsequently send signals to osteoblasts to lay down new bone mineral.[2] Maintenance of skeletal homeostasis relies on this delicate balance of bone resorption coupled with bone formation during remodeling. An imbalance in this process ultimately leads to bone disorders such as osteoporosis and Paget's disease.[3] Currently, RANKL inhibitors (e.g., Denosumab) and bisphosphonates are the primary drug treatments used to treat osteoporosis; however, their use associates with adverse effects, including microfractures, atypical femoral fractures, and osteonecrosis of the jaw.[4] The development of new drugs specifically targeting regulatory pathways may ultimately lead to better treatment of osteoporotic patients. Greater understanding of transcriptional control orchestrating osteoclastogenesis and activity is needed to preserve the quality of life for those with osteoporosis. Epigenetic regulators represent major orchestrators of gene expression control; thus, elucidation of their functions within osteoclasts may yield new therapeutic avenues.[5]

Epigenetics is the study of changes in gene expression that can be heritable or a result of environmental factors that do not change DNA sequences themselves.[6] The main forms of epigenetic modifications are histone protein modifications, DNA methylation, and short non-coding RNA sequences.[5] The histone proteins H2A, H2B, H3, and H4 can all be modified via addition or removal of acetyl, methyl, phospho, sumo, or ubiqityl groups to either upregulate or downregulate gene expression.[6] One major benefit to studying epigenetic regulators that makes this class of enzymes desirable targets is that they control reversible chromatin modifications.[6] In fact, many drugs affecting epigenetic regulators have already been developed, FDA approved, and shown to be clinically effective.[6] Thus, the importance of studying these epigenetic regulators is quite relevant.

Lysine specific demethylase 1 (LSD1 or KDM1A) is a member of the histone demethylases that functions by removing mono- or di- methyl groups from histone 3 lysine 4 (H3K4) or histone 3 lysine 9 (H3K9).[7] LSD1 as well as LSD2 differ from the other demethylase family members in that they require FAD binding to perform their demethylase activity. Removal of methyl groups from H3K4 results in decreased gene expression. In contrast, removal of methyl groups from H3K9 results in enhanced gene transcription; thus, LSD1 has a context dependent effect on gene expression.[7] Functions of LSD1 are well studied in many different cancers such as breast and prostate cancer; therefore, drugs that target LSD1 have already been developed and are being tested in human subjects.[8–10] The beneficial effects of LSD1-targeting drugs in animal models mimicking postmenopausal osteoporosis or rheumatoid arthritis have been tested with promising results suggesting LSD1 inhibitors may have promise in treating humans with these diseases.[11–13] Prior studies established that conditional deletion of *Lsd1* in osteoblasts resulted in increased osteoblast differentiation and mineralization ability via the upregulation of WNT7B and BMP2 expression[14]; however, the role of LSD1 in osteoclast differentiation and activity is currently not well understood.

In this study, we sought to understand how conditional deletion of *Lsd1* affects osteoclast differentiation. We show that deletion of *Lsd1* using the *LysM-cre* or *Cfms-cre*, targeting cells in the myeloid lineage or macrophage/osteoclast precursors, results in decreased osteoclast differentiation

Table 1. Genotyping primers.

Gene	5' ➔ 3' Primer
Lsd1	F: GCTGGATTGAGTTGGTTGTG R: CTGCTCCTGAAAGACCTGCT
LysM-Cre	F: TCCAATTTACTGACCGTACACCAA R: CCTGATCCTGGCAATTTCGGCTA
Cfms-Cre	F: CAGGGCCTTCTCCACACCAGCTG R:CTGGCTGTGAAGACCATCCAACAGCAC

and activity with a corresponding increase in bone mass in mice. Our results, together with previously published work in osteoblasts, suggest that LSD1 inhibitors may be a beneficial treatment for patients that suffer from osteoporosis.

Materials and methods

Ethics

All animal experiments were performed in accordance with institutional guidelines by the Institutional Animal Care (IACUC, protocol# 2104-39006A) and the Committee of the Office for the Protection of Research Subjects at the University of Minnesota, Minneapolis.

Lsd1 mice

Mice always had access to standard rodent chow and water and were housed in groups of 4-5. The housing room is maintained on a 14:10 hour light: dark cycle with controlled temperature and humidity. *Lsd1* floxed mice on a C57BL/6 background were obtained from Jackson Laboratories (strain # 023969, Bar Harbor, ME) via Dr. Stuart Orkin's laboratory (Harvard University, Boston, ME). *Lsd1* floxed mice were crossed with D2.129P2(B6)-Lyz2$^{tm1(cre)tfo}$/SjJmice (LysM-cre) (Jackson Laboratories, strain #026861) which have Cre-recombinase expressed in myeloid cells which includes osteoclasts or FVB-Tg (Csf1r-icre)1JWP/J (Jackson Laboratories, strain #021024), which includes macrophages, dendritic cells, and osteoclasts. Information on mouse strains is included in Table S1. Sex and aged match littermate mice were examined in our analysis. Genotyping primers for *Lsd1$^{fl/fl}$* mice listed in Table 1.

In vitro osteoclast analyses

Primary osteoclast culture

Femora and tibiae were dissected from *Lsd1$^{fl/fl}$* (Lsd1WT), *Lsd1$^{fl/fl}$ LysM-cre^{+}* (Lsd1LysmcKO), or *Lsd $^{fl/fl}$ Cfms-Cre^{+}* (Lsd1CfmsKO) and all adherent tissues were removed. Femora were saved for micro-CT and histology analyses. Primary bone marrow cells were isolated from the tibiae by flushing the marrow cavity with osteoclast media (phenol red-free alpha-MEM (Gibco, catalog #41061-037) with 25 units/mL penicillin/streptomycin (Invitrogen, catalog #15140-122), 400 mM L-Glutamine (Invitrogen, catalog #SH30034.01), and 5% fetal bone serum (Atlanta Biologicals). Red blood cells from the marrow sample were lysed using a Red Blood Cell lysis buffer (10 mM $KHCO_3$, 150 mM NH_4Cl, 0.1 mM EDTA pH 7.4). The remaining cells were cultured in 10 cm tissue culture dishes overnight (TPP brand tissue culture test plate, MidSci) in osteoclast media supplemented with 1.5% CMG 14-12 (cell culture supernatant containing M-CSF, Dr. Sunao Takeshita, Nagoya City University, Nagoya, Japan). CMG 14-12 is a mouse cell line that expresses high levels of M-CSF.[15] Non-adherent cell populations in the supernatant were collected and replated in 12-well cell culture plates (TPP brand tissue culture plate, MidSci) at a concentration of 2×10^5 cells per well in osteoclast media supplemented with 1.5% CMG 14-12 conditioned media. Cell cultures were subsequently supplemented every 2 d with 1.5% CMG 14-12 conditioned media and 5 ng/mL of RANKL (R&D Systems, catalog #463-TEC) to induce osteoclastogenesis.

For interferon-β (IFN-β) inhibition studies, Lsd1Cfms-cKO osteoclast cultures from male mice were treated with 30 units/mL of neutralizing anti-mouse IFN-β antibody (R and D Systems, catalog #32400-1) or isotype control anti-rabbit IgG antibody (R and D Systems, catalog # AB105-C) at the time of RANKL differentiation as previously described.[16] Antibodies were replaced every 2 d with replacement of differentiation media.

TRAP and DAPI staining

Differentiated osteoclasts were rinsed with 1X DPBS (Gibco) and fixed with 4% paraformaldehyde (Thermo Scientific) for 20 min. Osteoclasts expressing TRAP were stained using the Naphthol AS-MX phosphate and Fast Violet LB salt protocol (BD Biosciences Technical Bulletin #445). Osteoclasts were imaged and photographed using light microscopy. Images were analyzed using NIH ImageJ to measure the number and size of TRAP positive osteoclasts. Cells were then stained with 0.1% DAPI dye (ThermoFisher, Catalog #D1306) in PBS for 10 min. in the dark at room temperature. Cells were imaged and photographed using fluorescent microscopy. Nuclei were quantified using NIH ImageJ.

Bone resorption assay

Primary bone marrow cells were plated on Osteo Assay surface plates (Corning, catalog #CLS3987) at a concentration of 100,000 cells per well and allowed to fully differentiate. Cells were initially plated with osteoclast media supplemented with 1.5% CMG 14-12 conditioned media and subsequently given osteoclast media at a pH of 6.8 supplemented with 1.5% CMG 14-12 conditioned media and 5 ng/mL of RANKL every 2 d. After 7 d of RANKL stimulation, media was aspirated off and 10% bleach was added to each well and allowed to sit for 10 min at room temperature. The bleach solution was removed, and each well was washed with dH_2O twice and allowed to dry at room temperature. Plates were imaged and photographed using light microscopy. Resorption pits were analyzed using NIH ImageJ.

Bulk RNA-SEQ

Bone marrow cells were collected from 3-mo female Lsd1LysM-WT and Lsd1LysM-cKO and differentiated in M-CSF (CMG 14-12 supernatant) only or M-CSF and RANKL for 2 d. Cells were lysed and total RNA collected using RNA Plus Mini Kit (Qiagen, catalog #74134) following manufacturer's instructions. High throughput RNA sequencing was performed by the UMN Genomics Center. 2×50 bp FastQ paired end reads for 6 samples (n = 62.1 million average reads per sample) were trimmed using Trimmomatic (v 0.33) enabled with the optional "-q" option; 3 bp sliding-window trimming from 3' end requiring minimum Q30. Quality control on raw sequence data for each sample was

Table 2. RT-qPCR primers.

Gene	5' ➔ 3' Primer
Lsd1	F: ATGGATGTCACACTTCTGGA
	R: CAAGACCTGTTACAACCATG
Fos	F: CCAAGCGGAGACAGATCAACTT
	R: TCCAGTTTTTCCTTCTCTTTCAGCAGA
Nfatc1	F: TCATCCTGTCCAACACCAAA
	R: TCACCCTGGTGTTCTTCCTC
Dcstamp	F: GGGCACCAGTATTTTCCTGA
	R: TGGCAGGATCCAGTAAAAGG
Ctsk	F: AGGGAAGCAAGCACTGGATA
	R: GCTGGCTGGAATCACATCTT
Hprt	F: GAGGAGTCCTGTTGATGTTGCCAG
	R: GGCTGGCCTATAGGCTCATAGTGC
Ifit1	F:CAACTGAGGACATCCCGAAACA
	R:ATGTGGGCCTCAGTTTCAAAGT
Irf7	F: GAGCGAAGAGAGCGAAGAGG
	R:GCCCCACAGTAGATCCAAGC
Tlr3	F:CCTCCAACTGTCTACCAGTTCC
	R:GCCTGGCTAAGTTATTGTGC
Tlr5	F:AGCATTCTCATGGTGGTGG
	R:AATGGTTGCTATGGTTCGC
Cxcl10	F:AGTGCTGCCGTCATTTTCTG
	R:ATTCTCACTGGCCCGTCAT
Oasl2	F:AGGGGACAACCCTGAACCA
	R:TAGGCCAGGCTTCTGCTACA
Ifn-β	F:AGGGCGGACTTCAAGATC
	R:CTCATTCCACCCAGTGCT

performed with FastQC. Read mapping was performed via Hisat2 (v2.1.0) using the mouse genome (GRCm38 v94) as reference. Gene quantification was done via Feature Counts for raw read counts. Differentially expressed genes (DEGs) were identified using the edgeR (negative binomial) feature in CLCGWB (Qiagen, Redwood City, CA) using raw read counts. We filtered the generated list based on a minimum 2x Absolute Fold Change and FDR corrected $p<.05$. Data are deposited in GEO accession number GSE245698. Differential pathway analysis was performed using DAVID analysis.[17,18] Heatmap was plotted by http://www.bioinformatics.com.cn/srplot, an online platform for data analysis and visualization.

Real time quantitative PCR analysis

RNA was isolated and purified using Trizol (Thermo Fisher, catalog #15596018) extraction and quantified using a nanodrop spectroscopy. cDNA was prepared from 1 ug of purified RNA using the iScript cDNA Synthesis Kit (Bio-Rad, catalog #1708891) as stated in the manufacturer's protocol. Each reaction contained 500 nM of both the forward and reverse primers, 10 μL of iTaq Universal Sybr Green Supermix (Bio-Rad, catalog #1725121), 8.8 μL DEPC H_2O (Ambion, catalog #AM9906), and 1 μL of cDNA. The RT-qPCR protocol is as follows: 95°C for 3 min, 40 cycles of 94°C for 15 s, 58°C for 30 s, and 72°C for 30 s. Melting curve analysis followed: 95°C for 5 s, 65°C for 5 s, and lastly 65°C to 95°C with 0.5°C increments for 5 s each. The forward and reverse primer pairs for each gene are shown in Table 2.

Immunoblotting

Protein lysates were harvested from osteoclasts using modified RIPA buffer (150 mM NaCl, 0.25% sodium deoxycholate, 50 mM Tris pH 7.4, 1% IGEPAL, 1 mM EDTA) supplemented with Halt Protease & Phosphatase Inhibitor Cocktail (Thermo Scientific, catalog #78445). Lysates were purified by centrifugation at 17000 X g at 4°C. Proteins were resolved by SDS-PAGE and transferred to PVDF membrane (Millipore, catalog #IPVH0010). Membranes were incubated overnight with primary antibodies (antibody list shown in Table S2). HPR-conjugated anti-rabbit (GE Healthcare, catalog #NA934) or anti-mouse (GE Healthcare, catalog #GENA931) was incubated with membranes, washed, and developed using Western Bright Quantum (Advansta, catalog #K12042D10) detection agent. Images were acquired using BioRad Chemitouch.

Immunoprecipitation

Bone marrow cells were isolated as described above. Non-adherent cell populations in the supernatant were collected and replated in 10 cm cell culture plates (TPP brand tissue culture plate, MidSci) at a concentration of 5×10^6 cells per plate in osteoclast media supplemented with 1.5% CMG 14-12 conditioned media. Cell cultures were subsequently supplemented every 2 d with 1.5% CMG 14-12 conditioned media only or 1.5% CMG 14-12 conditioned media and 30 ng/mL of RANKL to induce osteoclastogenesis. Cells were harvested by scaping cells off plates with PBS. Cells were then lysed using Pierce IP Lysis Buffer (Thermo Scientific, catalog #87787) supplemented with Halt Protease & Phosphatase Inhibitor Cocktail. Lysates were purified by centrifugation at 13000 rpm for 10 min at 4°C. 10% of the lysate was collected for IP input and the rest of the lysate was split up evenly to be incubated with 5 μg of antibody overnight. EZview Red Protein G beads (Sigma-Aldrich, catalog #E3403) were washed and centrifuged at 5000 rcf for 1 min twice. Lysate and antibody mixes were then allowed to rotate and incubate with beads for 2 hours at 4°C. Beads were centrifuged at 5000 rcf for 1 min and supernatant was removed. Beads were subsequently washed with PBS and centrifuged thrice. Immunoblotting using the beads diluted in PBS was performed following the above protocol.

In vivo bone analyses

Micro-computed tomography analysis

Three-month-old femora were isolated, wrapped in gauze, and stored in PBS at −80°C. At the time of scanning, femora were defrosted to room temperature and scanned in PBS with a 1 mm aluminum filter using a XT H 225 micro-computed tomography machine (Nikon Metrology Inc., Brighton, MI, United States) at an isotropic voxel size of 7.11 μm. Scan settings were set to 120 kV, 61 μA, 720 projections, 2 frames per projections and integration time of 708 ms. 3D reconstruction volumes were made for each scan using CT Pro 3D (Nikon Metrology Inc., Brighton, MI, United States). These 3D volumes were then converted to bitmap datasets using VGStudio MAX 3.2 (Volume Graphics GmbH, Heidelberg, Germany). Scans were rotated using DataViewer (SkyScan, Bruker microCT), prior to analysis. SkyScan CT-Analyzer was used to perform Morphometric analyses following Bruker's instructions and guidelines for the field.[19] The trabecular bone analysis was performed in the distal metaphysis starting 0.5 mm proximal to the growth plate and extended 1.5 mm proximally toward the diaphysis. The cortical bone analysis was a 0.5 mm section at the mid-diaphysis. Automated contouring was used in the region of interest for both trabecular and cortical bone with some manual editing as needed for each

sample. Global thresholding was used to remove surrounding tissue from analysis in both 3D trabecular and 2D cortical analyses.

Paraffin-embedded section staining

Three-month-old femora were isolated and fixed in Z-fix (Anatech LTD, catalog #NC9378601) and placed in 10% EDTA (pH 7.4) for decalcification, paraffin-embedded sectioning, and histological staining. Bone sections were then de-paraffinized using xylenes and rehydrated via an ethanol gradient. Sections were then TRAP stained using the above protocol at 37°C for 1 hour. Sections were counterstained with methyl-green for 15 seconds and prepared for imaging using permount mounting media, cover slipped, and allowed to dry for 24 hours. Images were taken using light microscopy and analyzed using NIH image J.

Statistical analysis

All results are expressed as means with standard deviations. For all in vitro experiments, graphs represent an average of at least 3 independent experiments performed in triplicate. The in vivo data represent all the samples gathered graphed together. None of the samples were removed as outliers. Student t-tests were used for all experiments. All statistical analyses were performed using GraphPad Prism 8.

Results

Lsd1cKO mice have increased bone mass

To study the role of LSD1 in regulating osteoclast differentiation, we initially created a mouse model by crossing *LysM-cre* mice with $Lsd^{fl/fl}$ mice to create $Lsd1^{fl/fl}$ (herein referred to as Lsd1LysM-WT) and $Lsd^{fl/fl}$ *LysM-cre* (herein referred to as Lsd1LysM-cKO) mice. Three-month-old mice were used to determine the in vivo skeletal phenotype of male and female Lsd1LysM-cKO mice as compared to their sex-matched littermate controls. 3D reconstruction and volumetric analysis using micro-computed tomography (μCT) revealed that Lsd1LysM-cKO female, but not male mice, have significantly more trabecular bone volume to total volume (BV/TV, compare WT 3.993 vs LysM-cKO 4.889) compared Lsd1LysM-WT mice (Figure 1A-B, F-G). Furthermore, Lsd1LysM-cKO females but not males have significantly more trabeculae (Tb.N, compare WT 1.295 vs LysM-cKO 1.544) and less trabecular spacing (Tb.Sp, compare WT 0.211 vs LysM-cKO 0.1919), (Figure 1C-E, H-J) compared to Lsd1LysM-WT mice. When analyzing the cortical phenotype of these mice, the female Lsd1LysM-cKO mice have a significant increase in mean total cross sectional tissue area (T.Ar) and tissue perimeter (T.Pm) (Figure 1O-P); however, female mice did not have any significant changes in the other cortical parameters (Figure 1L-N). Male Lsd1LysM-cKO mice did not have any significant changes in any of the cortical parameters (Figure 1Q-V). Together, these results demonstrate that Lsd1LysM-cKO female mice have increased bone mass, but that loss of *Lsd1* in the myeloid lineage does not significantly affect the trabecular or cortical parameters of the male skeleton.

Since *LysM-Cre* targets myeloid lineage cells and not just osteoclast precursors, we chose to analyze the skeletal phenotype of $Lsd1^{fl/fl}$ mice bred to the *Cfms-Cre* mouse strain. *Cfms-Cre* targets macrophage, osteoclast precursors, and dendritic cells.[20] We have previously used this *Cre* expressing mouse line to conditionally delete genes such as *Hdac7*, *Mef2a,* and *Mef2c* from osteoclast precursors.[21–23] $Lsd1^{fl/fl}$ mice were bred to *Cfms-cre* expressing mouse line to generate $Lsd1^{fl/fl}$ (Lsd1Cfms-WT) and $Lsd1^{fl/fl}$*;Cfms-cre* (Lsd1Cfms-cKO) mice and their sex-matched littermate controls. Similar to our analysis with the *LysM-Cre* mice, 3-mo-old mice were used to determine the in vivo skeletal phenotype of male and female Lsd1Cfms-cKO mice. Unlike Lsd1LysM-cKO mice, micro-CT analysis revealed that male not female mice had significantly more trabecular bone volume to total volume (BV/TV compare Lsd1Cfms-WT 13.14 vs Lsd1Cfms-cKO 15.20) compared to Lsd1Cfms-WT mice (Figure 2A-B, F-G). Male Lsd1Cfms-cKO mice also demonstrated a significantly enhanced trabecular number (Tb.N, compare Lsd1Cfms-WT 2.252 vs Lsd1Cfms-cKO 2.699), with a corresponding decrease in thickness (Tb.Th, compare Lsd1Cfms-WT 0.05842 vs Lsd1Cfms-cKO 0.05642). Lastly, while not significant, male mice exhibited diminished trabecular spacing (Tb.Sp, compare Lsd1Cfms-WT 0.2286 vs Lsd1Cfms-cKO 0.2115) (Figure 2C-E, H-J). Both male and female Lsd1Cfms-cKO mice had significantly more cortical bone volume to total volume (Male BV/TV, compare Lsd1Cfms-WT 49.96 vs Lsd1Cfms-cKO 51.16, Female BV/TV, compare Lsd1Cfms-WT 48.06 vs Lsd1Cfms-cKO 50.11, Figure 2L and R), but no other cortical parameters were significantly affected (Figure 2M-V). These data demonstrate that conditional deletion of *Lsd1* within *Cfms-cre*-expressing cells enhances attainment of peak trabecular bone mass in male mice and cortical bone in both male and female mice.

Lsd1cKO osteoclasts have decreased differentiation and activity

To determine the in vitro phenotype of osteoclasts derived from Lsd1LysM-cKO and Lsd1Cfms-cKO mice, we initially confirmed significantly decreased LSD1 expression by qRT-PCR and western blot (Figures 3A and 4A, Figure S1A-B). As we detect significantly decreased expression of LSD1 RNA and protein in our M-CSF only cultures (day 0), these data indicate that both *LysM* and *Cfms-Cre* drivers are active at this time point during osteoclast differentiation. To measure osteoclast formation in vitro, we stimulated bone marrow cells from LSD1LysM-WT and -cKO mice with M-CSF and RANKL for 48 hours (day 2) and 72 hours (day 3). TRAP-stained images show that there are significantly less TRAP positive osteoclasts at days 2 and 3 of differentiation (Figure 3B-D). Additionally, at day 3 of differentiation Lsd1LysM-cKO osteoclasts are approximately 20-fold smaller in size compared to Lsd1LysM-WT (from both male and female mice, Figure 3E-F). Similar results were seen with bone marrow cells isolated from male and female LSD1Cfms-WT and -cKO mice (Figure 4B-F).

To determine if the decrease in size of the TRAP positive osteoclasts was due to the inability to proliferate, osteoclast cultures from female Lsd1LysM-WT and Lsd1LysM-cKO mice were stained with DAPI to quantify the number of nuclei present. RANKL has been reported to transiently increase proliferation of bone marrow macrophages before resulting in arrest of cell proliferation.[24] At day 2 of differentiation there was no significant difference between the number of nuclei. In contrast, at day 3 of differentiation

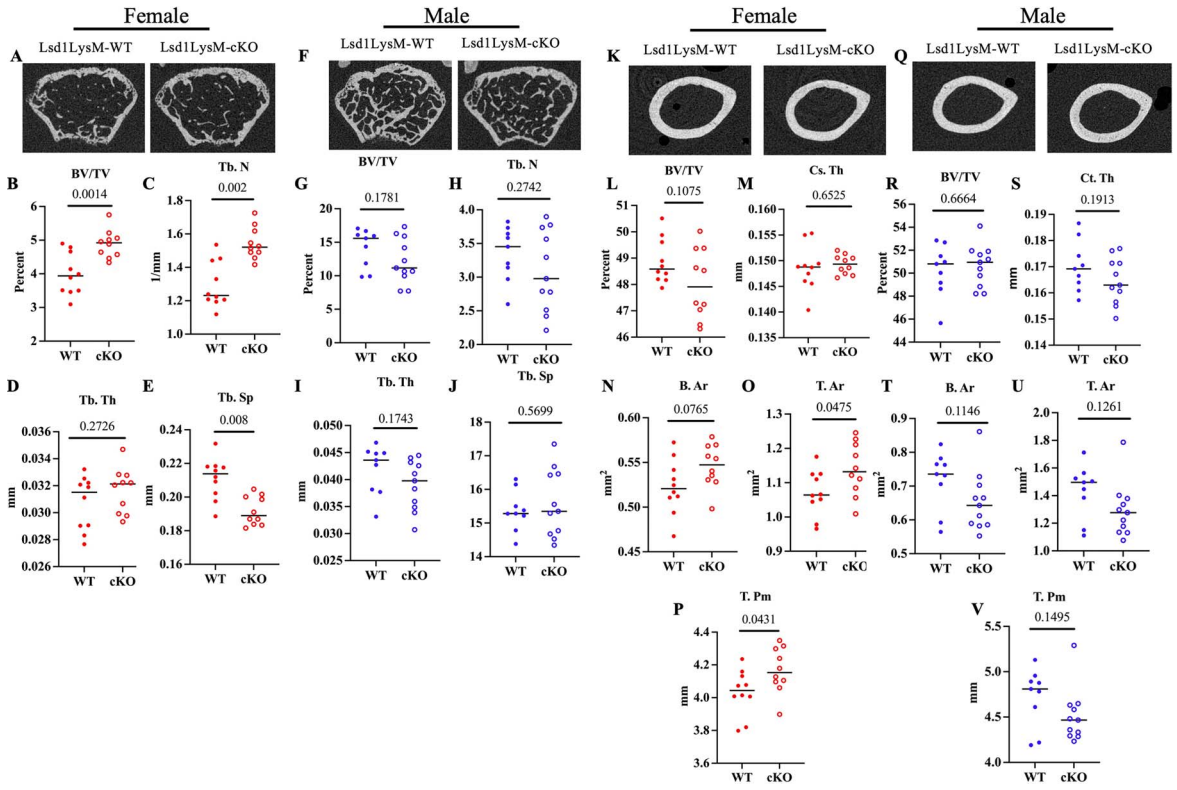

Figure 1. Female Lsd1LysM-cKO mice have increased bone mass at 3 months of age. Representative trabecular micro-CT images of female (A) and male (F) Lsd1LysM-WT and Lsd1LysM-cKO mice. Measurements of (B and G) trabecular bone volume to total volume, (C and H) trabecular number, (D and I) trabecular thickness, (E and J) trabecular spacing are displayed. Female WT $n = 10$, female cKO $n = 10$, male WT $n = 9$, male cKO $n = 11$. Representative cortical micro-CT images of female (K) and male (Q) Lsd1LysM-WT and Lsd1LysM-cKO mice. Measurements of cortical bone volume to total volume, (L and R) cortical thickness, (M and S) mean total cross sectional bone area, (N and T) mean total cross sectional tissue area (O and U), and (P and V) mean total cross sectional tissue perimeter are displayed. Female WT $n = 10$, female cKO $n = 10$, male WT $n = 9$, male cKO $n = 11$. Individual p values are as shown.

there were in fact more nuclei present in the Lsd1LysM-cKO cultures (Figure S2A-B). Additionally, we were able to confirm an increase in *E2f* expression in Lsd1LysM-cKO osteoclasts as was previously reported[12] (Figure S2C). These data suggest that osteoclast differentiation is not inhibited in the Lsd1LysM-cKO mice due to the loss of osteoclast precursors.

To measure the ability of osteoclasts to demineralize, we plated the osteoclasts on calcium phosphate coated plates to measure their ability to resorb mineral. As expected, based on their decreased size, female Lsd1LysM-cKO osteoclasts were not able to effectively resorb as much mineral as their wildtype counterparts (2-fold decrease, Figure S3). Lastly qRT-PCR analysis shows that the loss of LSD1 results in a significant decrease in the osteoclast gene markers *Nfatc1*, *Dcstamp*, and *Ctsk*, but no significant change in *c-Fos* expression in pre-osteoclasts from Lsd1Cfms-cKO mice (Figure S4). These results signify that there is a decrease in genes that regulate osteoclast differentiation and activity in the absence of LSD1. Our RT-qPCR demonstrates that Lsd1Cfms-cKO osteoclasts had no change in *c-Fos*, but significantly diminished *Nfatc1* expression suggesting that LSD1 regulates genes involved in osteoclast differentiation after the commitment phase.

Lsd1cKO mice have decreased osteoclast surface per bone surface

To determine if changes seen in vitro are also seen in vivo osteoclast differentiation, we performed histological analysis of paraffin embedded bones. Our analysis demonstrated that female Lsd1LysM-cKO mice do not have a significant difference in the number of TRAP positive osteoclasts but do have approximately 2-fold decrease in percent of osteoclast surface per bone surface compared to female Lsd1LysM-WT mice (Figure 3G and I). In vivo analysis of the male Lsd1LysM-cKO bone sections exhibits no significant difference in the number of TRAP positive osteoclasts or percent osteoclast surface/bone surface (Figure 3H and J). We also performed histological analysis of bones from Lsd1Cfms-WT and -cKO mice. Male bone sections from Lsd1Cfms-cKO had both a 3-fold reduction in number and percent osteoclast surface per bone surface compared to bone sections from Lsd1Cfms-WT mice (Figure 4G and I). Female Lsd1Cfms-cKO mice had no significant change in either histological parameter (Figure 4H and J).

Lsd1cKO osteoclasts have an increase in overall methylation at H3K4

To better understand the decrease in osteoclast differentiation in the Lsd1LysM-cKO mice, we determined the global methylation status of the 2 targets of LSD1: H3K4 and H3K9. Both day 0 (M-CSF only) and day 2 (M-CSF and RANKL) of osteoclast differentiation, there is an increase in global mono-methylation of H3K4 in the Lsd1LysM-cKO osteoclasts, but no difference in global mono-methylation of H3K9 at either day (Figure 3K-L, Figure S5). Greater methylation of H3K4 suggests that LSD1 inhibits gene transcription to regulate osteoclast differentiation.

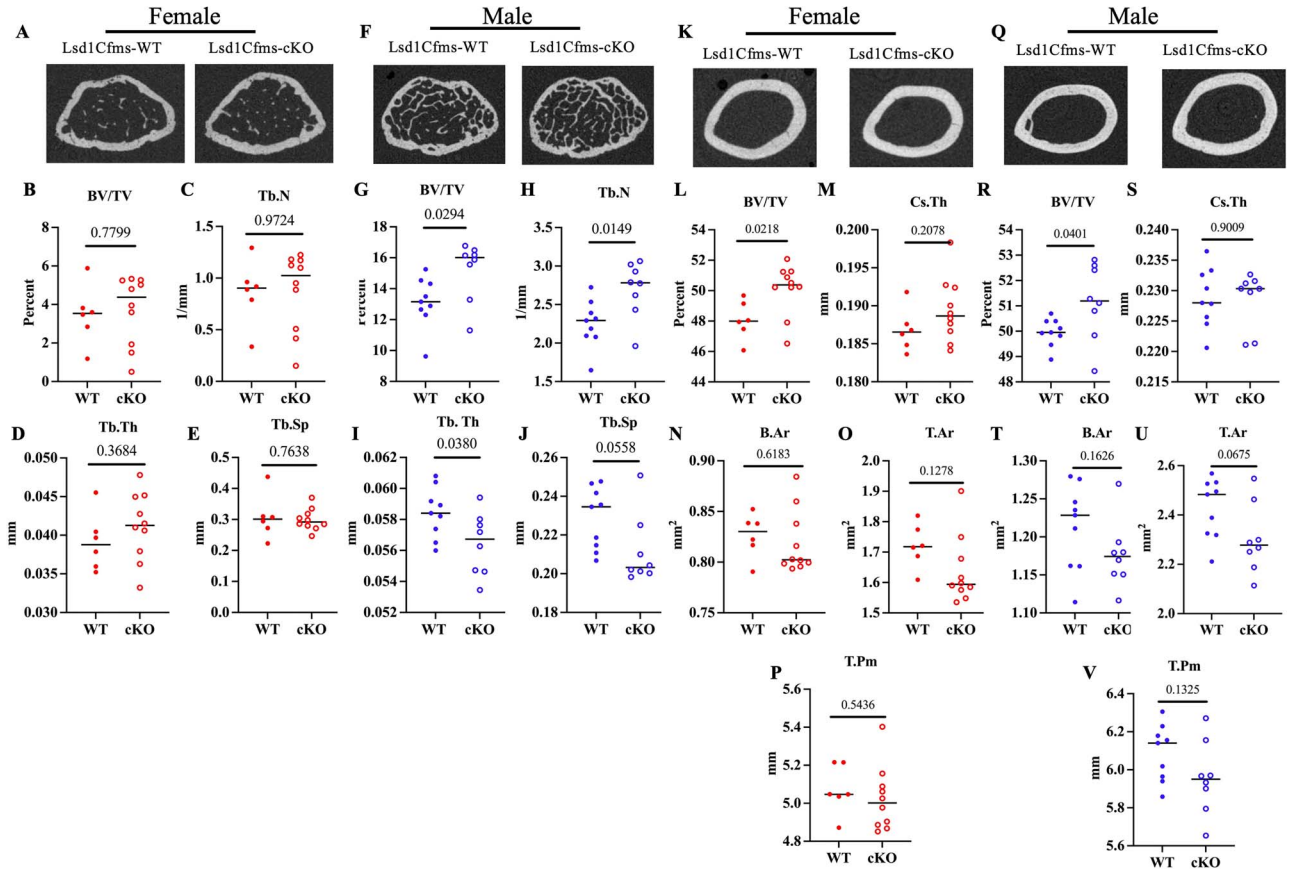

Figure 2. Male Lsd1Cfms-cKO mice have an increase bone mass at 3 mo of age. Representative trabecular micro-CT images of female (A) and male (F) Lsd1Cfms-WT and Lsd1Cfms-cKO mice. Measurements of (B and G) trabecular bone volume to total volume, (C and H) trabecular number, (D and I) trabecular thickness, (E and J) trabecular spacing are displayed. Female WT $n = 6$, female cKO $n = 9$, male WT $n = 8$, male cKO $n = 8$. Representative cortical micro-CT images of female (K) and male (Q) Lsd1Cfms-WT and Lsd1Cfms-cKO mice. Measurements of cortical bone volume to total volume, (L and R) cortical thickness, (M and S) mean total cross sectional bone area, (N and T) mean total cross sectional tissue area (O and U), and mean total cross sectional tissue perimeter (P and V) are displayed. Female WT $n = 6$, female cKO $n = 8$, male WT $n = 9$, male cKO $n = 8$. Individual p values are as shown.

Loss of LSD1 expression leads to increases in IFN-β regulated genes

We performed bulk RNA-sequencing of osteoclast precursors at day 0 (M-CSF only) or day 2 (M-CSF and RANKL) from Lsd1LysM-cKO males and females, as well as their sex-matched littermate controls to identify changes in gene expression due to the loss of LSD1 expression. The data shown are derived from female mice at day 2. Over 90% of the identified DEGs were up regulated in the Lsd1LysM-cKO cells (false discovery rate of 0.05 and fold change of greater than 2) which agrees with our results that LSD1 acts as a repressor (increase in H3K4me1 in Lsd1LysM-cKO osteoclast precursors (Figure 3I). Using DAVID analysis of DEGs, we determined up and down regulated pathways in Lsd1LysM-cKO versus Lsd1LysM-WT preosteoclasts (Figure 5B-C, Tables S3–S4). Genes involved in the IFN-β signaling pathway were upregulated in innate immunity, immunity and inflammation pathways in Lsd1LysM-cKO compared to Lsd1LysM-WT cells (Figure 5B).

IFN-β signaling negatively regulates osteoclast differentiation.[25] We validated significantly elevated expression of genes such as *Ifit1*, *Irf7*, *Oasl2*, *Cxcl10*, *Tlr3*, and *Tlr5* in both Lsd1LysM-cKO and Lsd1Cfms-cKO cells compared to wild type cells at both days 0 and 2 (Figure 5E-I, **data not shown**) via qRT-PCR. IFN-β signaling enhances expression of these genes in other cell types.[26] To determine if this is true within osteoclasts, cells were treated on either day 0 or day 2 with IFN-β for 3 hours. IFN-β stimulation significantly enhanced expression levels of these genes as compared to mock treated cells (Figure 5J-N). Our data suggest that one mechanism by which LSD1 regulates osteoclast differentiation is through downregulation of the genes involved in the IFN-β pathway.

Inhibition of IFN-β signaling restores osteoclast differentiation in Lsd1CfmsKO

Before blocking IFN-β signaling to determine if excess signaling was responsible for differences in differentiation seen in the osteoclasts lacking LSD1 expression, we determined if osteoclasts express IFN-β as previously reported.[27] Both days 0 and 2 preosteoclasts expressed levels of IFN-β as measured by qRT-PCR (Figure 5O). Next we added a neutralizing antibody against IFN-β, or an isotype control to male Lsd1Cfms-cKO osteoclast cultures at the time of RANKL addition. Lsd1Cfms-cKO cells treated with the IFN-β neutralizing antibody had significantly larger TRAP positive cells compared to cells treated with the isotype (Figure 5P). These data demonstrate that multinuclear cells formation is partially restored in Lsd1Cfms-cKO cell by blocking IFN-β signaling.

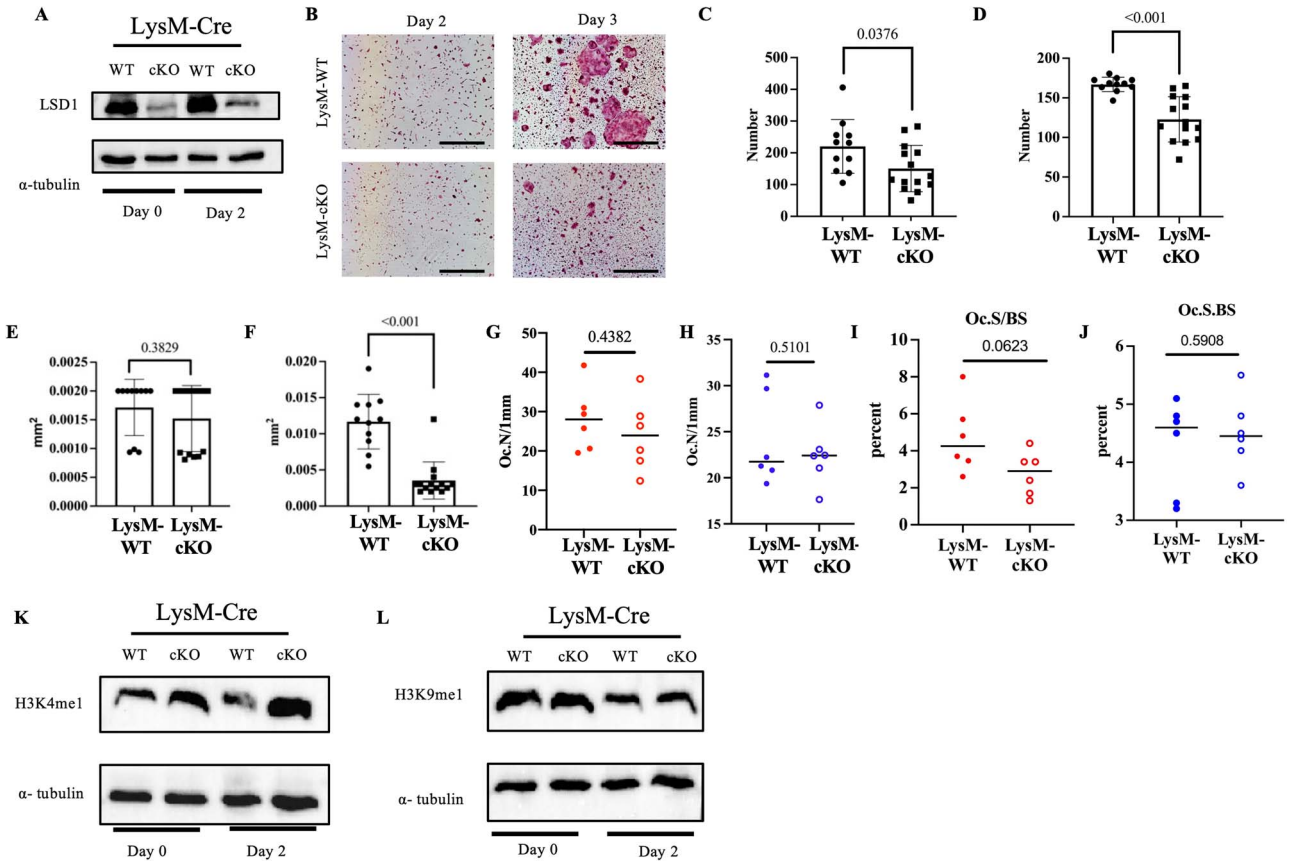

Figure 3. Lsd1LysM-cKO mice have smaller osteoclasts. Bone marrow cells from Lsd1LysM-WT and Lsd1LysM-cKO male and female mice were stimulated with M-CSF and RANKL to induce osteoclast differentiation. (A) Immunoblot of LSD1 expression in Lsd1LysM-WT and Lsd1LysM-cKO osteoclasts at day 0 (M-CSF only) and day 2 (M-CSF and RANKL). (B) Representative TRAP-stained images of cells 48 hours (day 2) and 72 hours (day 3) after RANKL stimulation. Scale bar = 0.5 um. (C) Average number of TRAP positive cells at 48 hours and (D) 72 hours after RANKL treatment (E) average size of TRAP positive cells at 48 hours and (F) 72 hours after RANKL treatment. (G-J) Quantification of TRAP positive cells in bone slices from LSD1LysM-WT and LSD1LysM-cKO mice. (G) Osteoclast number per bone surface in female mice. (H) Osteoclast number per bone surface in male mice. (I) Osteoclast surface to bone surface in female mice. (J) Osteoclast surface to bone surface in male mice $n = 6$ per genotype. Scale bar = 10 um. (K) Immunoblot analysis of mono-methylated H3K4 from female LSD1LysM-WT and LSD1LysM-cKO mice. (L) Immunoblot analysis of global mono-methylated H3K9me1 in osteoclast lysates from female Lsd1LysM-WT and Lsd1LysM-cKO at day 0 (M-CSF only) and day 2 (M-CSF and RANKL). Data presented represent at least 3 biological replicates. Individual *p* values are as shown. Abbreviations: LSD1, lysine specific demethylase 1; TRAP, tartrate-resistant acid phosphatase.

LSD1 can form a complex with HDACs 1 and 2

Many studies of LSD1 in other cell types demonstrate that LSD1 forms a complex with the corepressor CoREST (RCOR1) and histone deacetylases HDAC1 and HDAC2. These interactions facilitate LSD1-dependent demethylation of target genes.[28–30] To determine if this was indeed the case during osteoclast differentiation as well, we immunoprecipitated LSD1 in Lsd1LysM-WT and Lsd1LysM-cKO female osteoclast precursors and immunoblotted for HDAC1 and HDAC2. LSD1 is present within an immune complex containing HDAC1 and HDAC2 within osteoclast precursors stimulated with M-CSF only (Figure 6A, **left panel,** Figure S6). Importantly, when we attempt to immunoprecipitate LSD1 from Lsd1LysM-cKO osteoclasts, we see the loss of HDAC1 and HDAC2 binding (Figure 6A, right panel). These data demonstrate that LSD1 forms a complex containing HDAC1/2 within osteoclasts. We next determined if LSD1 depletion and associated loss of HDAC1/2 binding impacted the acetylation status of H3K9, a target for deacetylation by class I HDACs.[31,32] Interestingly, loss of LSD1 expression was associated with enhanced global acetylation of H3K9 in osteoclast precursors stimulated with M-CSF only (Figure 6B, Figure S6). However, we were unable to analyze changes in H4 acetylation by western blot so it is unclear if the changes we determined for H3K9 were specific or whether changes to LSD1 expression result in global changes to both H3 and H4 acetylation.

Discussion

An imbalance in bone remodeling due to increased osteoclast differentiation ultimately leads to bone related diseases such as osteoporosis and periodontal disease.[3] A better understanding of the molecular mechanisms that regulate osteoclast gene expression will help us recognize how these cells promote bone loss and can uncover new possible drug targets.[33] Epigenetic factors have shown to be drug targets for regulating gene expression in a plethora of cell types.[6] One of these factors, specifically in cancers, is LSD1.[8–10,34] However, to date, not much is known about the mechanisms by which LSD1 regulates gene expression during osteoclast differentiation.

In this study we show that conditional knockout of LSD1 in the myeloid lineage decreases the number and size of TRAP

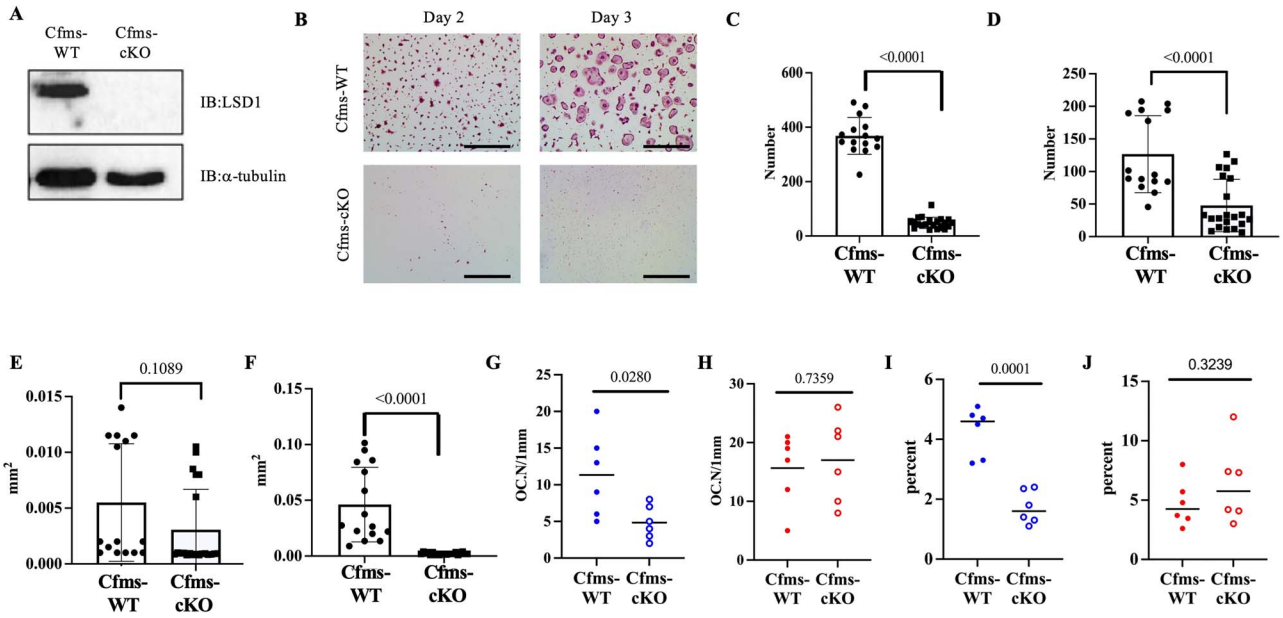

Figure 4. Lsd1Cfms-cKO mice have fewer and smaller TRAP positive osteoclasts. Bone marrow macrophages from male and female Lsd1Cfms-WT and Lsd1Cfms-KO mice were stimulated with M-CSF and RANKL to induce osteoclast differentiation. (A) Immunoblot of LSD1 expression in Lsd1Cfms-WT and Lsd1Cfms-cKO osteoclasts at day 2 after M-CSF and RANKL treated (B) Representative TRAP-stained images of cells 48 and 72 hours (day 3) after RANKL stimulation. Scale bar = 0.5 um. (C) Average number of TRAP positive cells at 48 hours and (D) 72 hours after RANKL treatment. (E) average size of TRAP positive cells at 48 hours and (F) 72 hours after RANKL treatment. (G-J) Quantification of TRAP positive cells in bone slices from Lsd1Cfms-WT and Lsd1Cfms-cKO mice. (G) Osteoclast number per bone surface in female mice. (H) Osteoclast number per bone surface in male mice. (I) Osteoclast surface to bone surface in female mice. (J) Osteoclast surface to bone surface in male mice $n = 6$ per genotype. Scale bar = 10 um. Data presented represent at least 3 biological replicates. Individual p values are as shown. Abbreviations: LSD1, lysine specific demethylase 1; TRAP, tartrate-resistant acid phosphatase

positive osteoclasts. To test these effects in vivo, we performed μCT to examine the effects on bone. We show that Lsd1LysM-cKO female mice have significantly more bone compared to their Lsd1LysM-WT littermates. Additionally, we show that Lsd1LysM-cKO female mice have a smaller percentage of osteoclasts per bone surface.

Previous studies have shown that LSD1 interacts with the estrogen receptor α (ERα) in breast cancer cells and may suggest a mechanism for the fact that we only measured a significant skeletal phenotype in female Lsd1LysM-cKO mice.[35] We attempted to confirm this interaction in osteoclasts by co-immunoprecipitation, however we have yet to confirm an interaction. Our data demonstrate that LSD1 promotes osteoclast differentiation while ER-α is a negative regulator of osteoclast differentiation.[36-38] Our inability to confirm an interaction with LSD1 and ER-α may indicate that this interaction is cell specific. Recently it has become apparent that metabolic reprogramming is necessary during osteoclast differentiation.[39–42] Our RNA-SEQ analysis indicated that expression of *estrogen related receptor* (*Err-α*) is downregulated in our Lsd1LysM-cKO mice. We were able to confirm reduced expression of *Err-α* by qRT-PCR (data not shown). In the Kiviranta et al. study of LSD1 regulation of osteoblast differentiation, their ChIP-SEQ indicated that LSD1 binds to DNA site near the *Err-α* locus. Previously it has been shown that the transcription factor myc along with *Err-α* drives metabolic reprogramming to an oxidative state during osteoclast differentiation.[43] Interestingly changes in metabolism have been linked to regulation of inflammatory responses of immune cells. In a study by Doi et al. using human osteoclast precursors they concluded that LSD1 metabolically regulates osteoclast differentiation in inflammatory environments.[12] Our results in combination with their results may suggest that LSD1 is a promising therapeutic target for inflammatory bone diseases such as periodontal disease or rheumatoid arthritis.[44]

Interestingly, in our Lsd1Cfms-cKO mice it was the male mice in which we determined increased bone volume to total volume. The difference between males and females in *LysM* and *Cfms-Cre* expressing mouse lines may suggest differences in the stage of osteoclast differentiation or the interaction of cells in which *Lsd1* is conditionally deleted with other cell types contributing to sex specific phenotypes. Another reason for the differences between the *LysM* and *Cfms* phenotypes may be that different strains of mice have different male and female skeletal phenotypes. The mixed background of our mice may have contributed to the differences that we see between male and female *LysM-Cre* and *Cfms-Cre* expressing mice.[45–47]

In both the *LysM-Cre* and *Cfms-Cre* models, the in vitro osteoclast phenotype was a decrease in osteoclast differentiation. To determine the mechanism by which LSD1 may be regulating osteoclast differentiation, we investigated the loss of LSD1 and osteoclast gene expression. The osteoclast gene markers *Nfatc1*, *Dcstamp*, and *Ctsk* were significantly downregulated in male Lsd1Cfms-cKO mice; however, we did not detect any significant difference in *c-Fos* expression in Lsd1Cfms-cKO osteoclasts. Additionally in both models we detected increases in genes involved in the IFN-β pathway. Previous studies have demonstrated that expression of IFN-β in osteoclasts is induced by c-FOS.[25] IFN-β then inhibits osteoclast differentiation by inhibiting the activity of c-FOS.[25] These data together suggest LSD1 positively regulates osteoclast differentiation by indirectly or directly regulating IFN-β

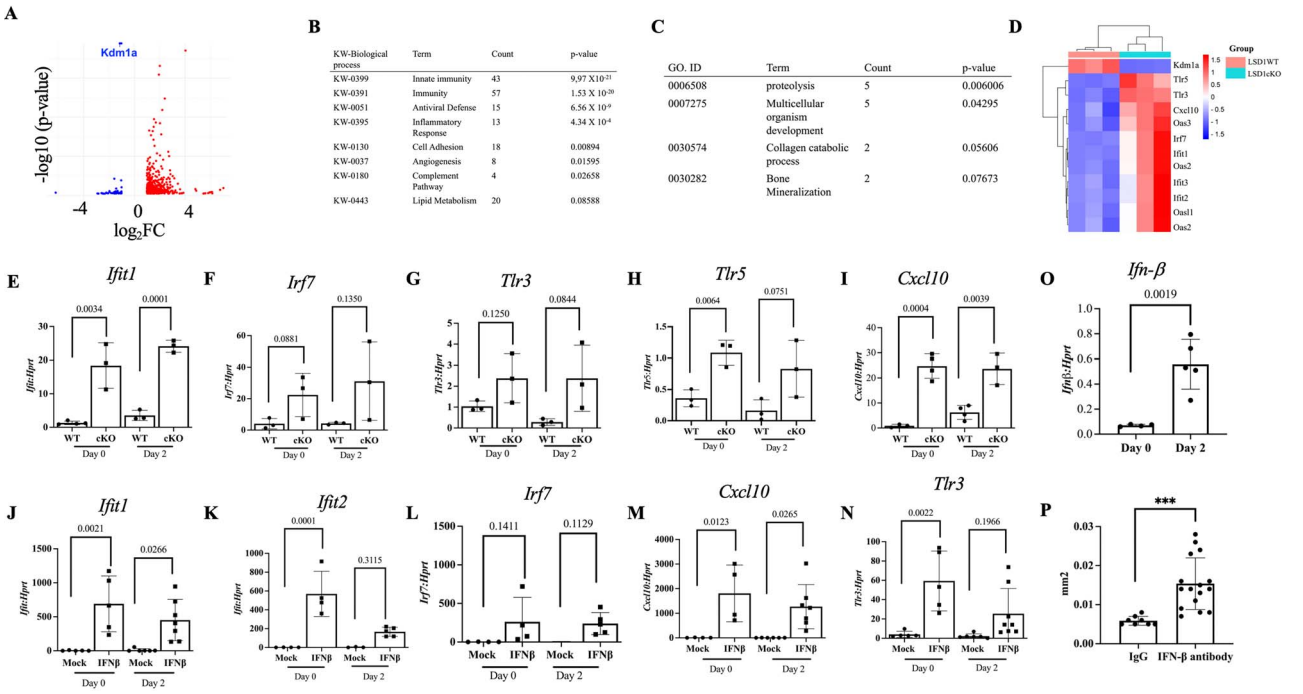

Figure 5. Lsd1LysM-cKO mice have increased expression of genes involved in the IFN-β pathway. (A) Volcano plot of number of differentially regulated genes identified by bulk RNA-SEQ from day 2 female Lsd1LysM-WT and -cKO osteoclast precursors. DAVID analysis of (B) biological processes upregulated and (C) downregulated in day 2 osteoclast precursors from female Lsd1LysM mice. (D) Heat map of IFN-β genes identified in bulk RNA-SEQ of Lsd1LysM-WT and Lsd1LysM-cKO osteoclast precursors. (E-I) qRT-PCR of selected IFN-β genes identified by RNA-SEQ at 0 or 48 hours after RANKL stimulation of female Lsd1LysM-WT and cKO osteoclast precursors. Individual p values are as shown. (J-N) qRT-PCR of selected IFN-β genes in WT cells treated with IFN-β (3×10^7 U/mg) for 3 hours. Data presented represent at least 3 biological replicates. Individual p values are as shown. (O) qRT-PCR of IFN-β expression in wild type osteoclast precursors at either day 0 (M-CSF only) and day 2 (M-CSF and RANKL). (P) Bone marrow cells were flushed from male Lsd1Cfms-cKO mice and at the time of RANKL addition either rabbit IgG or IFN-β neutralizing antibody, was added to cell cultures. Cells were cultured for 4 d in the presence of RANKL and antibody. Cell media and antibody was replaced every other day. Graph of average size of TRAP positive multinuclear cells. Data presented represent at least 3 biological replicates. Individual p values are as shown. Abbreviations: IFN-β, interferon-β; TRAP, tartrate-resistant acid phosphatase.

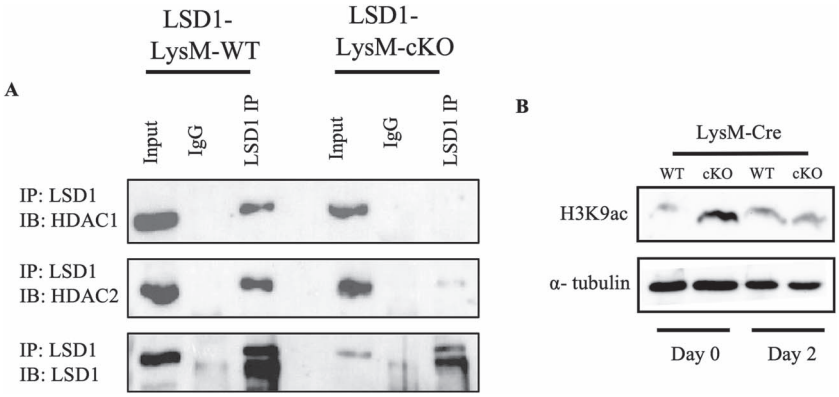

Figure 6. LSD1 can bind in a complex with HDAC1 and HDAC2. LSD1 was immunoprecipitated from osteoclast precursors from female Lsd1LysM-WT and -cKO mice. Immunoblotting analysis was performed to look for the presence of HDAC1, HDAC2, and LSD1 with M-CSF stimulation. (B) Immunoblot analysis of acetylated H3K9 0 hours and 48 hours after RANKL stimulation. Immunoblots were repeated with 3 biological replicates. Abbreviation: LSD1, lysine specific demethylase 1.

pathway genes during the early stages of osteoclast differentiation.

LSD1 targets histone residue H3K4me1 and H3K9me1, we see an increase in the amount of global H3K4me1 present in the Lsd1LysM-cKO osteoclasts. These data suggest that LSD1 may play a role in hindering osteoclast inhibitor gene expression via the removal of methylation from H3K4. Together with our bulk RNA-SEQ analysis, our data suggest that LSD1 activity restricts expression of IFN-β target gene allowing for osteoclast differentiation to proceed. Extending our analysis of our bulk RNA-SEQ beyond genes that have a fold change less than 2 but a p value <0.05, we identified epigenetic regulators including *Kdm1b*, *Kdm5b* and *Kdm5c*, *Dnmt3a*, and *Dotl1* that were differentially regulated in Lsd1LysM-cKO preosteoclasts (Table S5). These data suggest that expression of LSD1 may regulate expression of these epigenetic regulators or the inability of osteoclasts to differentiate in the absence of LSD1 expression may lead to downregulation

of these regulators. To confirm these changes further experiments such as chromatin immunoprecipitations, western blots to analyze changes in global histone modifications and qRT-PCR will need to be performed.

HDAC 1 and 2 was able to be co-immunoprecipitated with LSD1 at day 0 during osteoclast differentiation. Besides changes in total histone methylation, we also detected changes in histone acetylation levels in female Lsd1LysM-cKO osteoclasts. In other studies it has been suggested that HDACs may be important for LSD1's stability and demethylase function.[48] Inhibition of HDAC1 has been shown to suppress bone loss by inhibiting osteoclast differentiation in an arthritis mouse model or inflammatory cytokine production in human monocytes.[49] Suppression of both HDAC1 and 2 suppresses inflammatory cytokine expression and osteoclast resorption.[50] Future studies will determine targets of HDAC1, 2, and LSD1 during osteoclast differentiation and under inflammatory conditions such as periodontal disease.

Much of our data agree with a study determining the role of LSD1 in human osteoclasts.[12] Doi et al. showed that knockdown of LSD1 using shRNA in human osteoclasts suppresses differentiation and decreased pathological bone resorption in an arthritis mouse model.[12] They also demonstrated that RANKL stimulation induces LSD1 expression via the mTOR pathway.[12] While these results agreed with ours, the use of shRNAs in their study may cause off target effects and further studies would need to be performed to confirm their findings.

While much is still unknown about the role of LSD1 in osteoclast differentiation, it has been determined to be important in osteoblast differentiation. LSD1 regulates osteoblast differentiation by specifically targeting the genes *Wnt7b* and *Bmp2*.[14] The loss of *Lsd1* in both human mesenchymal stem cells (hMSCs) as well as mouse MSCs increased osteoblast differentiation and mineralization ability to increase bone volume.[14] Taken together, these data suggest that blocking LSD1 will decrease bone resorption and increase bone formation, making it an effective target for patients suffering from diseases such as periodontitis and osteoporosis. However, drug studies would need to be performed to confirm this.

To better understand how osteoclast differentiation may be inhibited, we are currently investigating the monocyte population in Lsd1LysM-WT and Lsd1LysM-cKO mice to determine if there are any differences in the cellular markers using flow cytometry. Though these experiments, we also hope to determine if changes in LSD1 expression and activity alters monocyte populations which may suggest how LSD1 regulates monocyte, macrophage, and osteoclast lineage commitment.

In conclusion, the loss of LSD1 in the myeloid lineage reduces the ability of osteoclasts to form and differentiate leading to an increase in bone volume in female mice.

Author contributions

Kristina Astleford-Hopper (Conceptualization, Data curation, Formal analysis, Writing—original draft, Writing—review & editing), Juan E. Abrahante Llorens (Formal analysis, Methodology, Writing—review & editing), Elizabeth Bradley (Formal analysis, Writing—review & editing), and Kim Mansky (Conceptualization, Formal analysis, Funding acquisition, Writing—original draft, Writing - review & editing). K.A.H. contributed to conception, design, data acquisition and interpretation, drafted and critically revised the manuscript. J.L. contributed to analysis of RNA-SEQ data. E.B. contributed to design, interpretation, and critically revised the manuscript. K.M. contributed to conception, design, data acquisition and interpretation, drafted, and critically revised the manuscript. All authors gave final approval and agreed to be accountable for all aspects of the work.

Supplementary material

Supplementary material is available at *JBMR Plus* online.

Funding

The authors disclosed receipt of the following financial support for the research, authorship, and/or publication of this article: MinnCResT Fellowship: T90 DE022732/R90, DE023058, and F30DE030354 to K.A.H. This study was supported by bridge funding to K.C.M. from the University of Minnesota School of Dentistry. Graphical Abstract was created in BioRender. Mansky, K. (2024) https://BioRender.com/x28g113

Conflicts of interest

None declared.

Data availability

The bulk RNA-SEQ data in this article are deposited in GEO at https://www.ncbi.nlm.nih.gov/geo/ and can be accessed with accession number GSE245698. The rest of the data underlying this article are available in this article and its online supplemental material.

References

1. Karsenty G, Wagner EF. Reaching a genetic and molecular understanding of skeletal development. *Dev Cell*. 2002;2(4):389-406. https://doi.org/10.1016/S1534-5807(02)00157-0
2. Raggatt LJ, Partridge NC. Cellular and molecular mechanisms of bone remodeling. *J Biol Chem*. 2010;285(33):25103-25108. https://doi.org/10.1074/jbc.R109.041087
3. Feng X, McDonald JM. Disorders of bone remodeling. *Annu Rev Pathol*. 2011;6(1):121-145. https://doi.org/10.1146/annurev-pathol-011110-130203
4. Kennel KA, Drake MT. Adverse effects of bisphosphonates: implications for osteoporosis management. *Mayo Clin Proc*. 2009;84(7):632-638. https://doi.org/10.1016/S0025-6196(11)60752-0
5. Husain A, Jeffries MA. Epigenetics and bone remodeling. *Curr Osteoporos Rep*. 2017;15(5):450-458. https://doi.org/10.1007/s11914-017-0391-y
6. Kelly TK, De Carvalho DD, Jones PA. Epigenetic modifications as therapeutic targets. *Nat Biotechnol*. 2010;28(10):1069-1078. https://doi.org/10.1038/nbt.1678
7. Hino S, Kohrogi K, Nakao M. Histone demethylase LSD1 controls the phenotypic plasticity of cancer cells. *Cancer Sci*. 2016;107(9):1187-1192. https://doi.org/10.1111/cas.13004
8. Vasilatos SN, Katz TA, Oesterreich S, Wan Y, Davidson NE, Huang Y. Crosstalk between lysine-specific demethylase 1 (LSD1) and histone deacetylases mediates antineoplastic efficacy of HDAC inhibitors in human breast cancer cells. *Carcinogenesis*. 2013;34(6):1196-1207. https://doi.org/10.1093/carcin/bgt033
9. Cao C, Wu H, Vasilatos SN, et al. HDAC5-LSD1 axis regulates antineoplastic effect of natural HDAC inhibitor sulforaphane in human breast cancer cells. *Int J Cancer*. 2018;143(6):1388-1401.
10. Sehrawat A, Gao L, Wang Y, et al. LSD1 activates a lethal prostate cancer gene network independently of its demethylase function. *Proc Natl Acad Sci USA*. 2018;115(18):E4179-E4188.

11. Ding M, Chen Z, Cho E, Park SW, Lee TH. Crucial role of lysine-specific histone demethylase 1 in RANKL-mediated osteoclast differentiation. *Int J Mol Sci*. 2023;24(4):3605. https://doi.org/10.3390/ijms24043605
12. Doi K, Murata K, Ito S, et al. Role of lysine-specific demethylase 1 in metabolically integrating osteoclast differentiation and inflammatory bone resorption through hypoxia-inducible factor 1alpha and E2F1. *Arthritis Rheumatol*. 2022;74(6):948-960. https://doi.org/10.1002/art.42074
13. Chen Z, Choi ER, Encarnacion AM, et al. Discovery of TCP-(MP)-caffeic acid analogs as a new class of agents for treatment of osteoclastic bone loss. *Bioorg Chem*. 2024;150:107603. https://doi.org/10.1016/j.bioorg.2024.107603
14. Sun J, Ermann J, Niu N, et al. Histone demethylase LSD1 regulates bone mass by controlling WNT7B and BMP2 signaling in osteoblasts. *Bone Res*. 2018;6(1):14. https://doi.org/10.1038/s41413-018-0015-x
15. Takeshita S, Kaji K, Kudo A. Identification and characterization of the new osteoclast progenitor with macrophage phenotypes being able to differentiate into mature osteoclasts. *J Bone Miner Res*. 2000;15(8):1477-1488. https://doi.org/10.1359/jbmr.2000.15.8.1477
16. Zheng H, Yu X, Collin-Osdoby P, Osdoby P. RANKL stimulates inducible nitric-oxide synthase expression and nitric oxide production in developing osteoclasts. An autocrine negative feedback mechanism triggered by RANKL-induced interferon-beta via NF-kappaB that restrains osteoclastogenesis and bone resorption. *J Biol Chem*. 2006;281(23):15809-15820.
17. Huang da W, Sherman BT, Lempicki RA. Systematic and integrative analysis of large gene lists using DAVID bioinformatics resources. *Nat Protoc*. 2009;4(1):44-57. https://doi.org/10.1038/nprot.2008.211
18. Sherman BT, Hao M, Qiu J, et al. DAVID: a web server for functional enrichment analysis and functional annotation of gene lists (2021 update). *Nucleic Acids Res*. 2022;50(W1):W216-W221. https://doi.org/10.1093/nar/gkac194
19. Bouxsein ML, Boyd SK, Christiansen BA, Guldberg RE, Jepsen KJ, Muller R. Guidelines for assessment of bone microstructure in rodents using micro-computed tomography. *J Bone Miner Res*. 2010;25(7):1468-1486. https://doi.org/10.1002/jbmr.141
20. Deng L, Zhou JF, Sellers RS, et al. A novel mouse model of inflammatory bowel disease links mammalian target of rapamycin-dependent hyperproliferation of colonic epithelium to inflammation-associated tumorigenesis. *Am J Pathol*. 2010;176(2):952-967. https://doi.org/10.2353/ajpath.2010.090622
21. Blixt N, Norton A, Zhang A, et al. Loss of myocyte enhancer factor 2 expression in osteoclasts leads to opposing skeletal phenotypes. *Bone*. 2020;138:115466. https://doi.org/10.1016/j.bone.2020.115466
22. Stemig M, Astelford K, Emery A, et al. Deletion of histone deacetylase 7 in osteoclasts decreases bone mass in mice by interactions with MITF. *PLoS One*. 2015;10(4):e0123843. https://doi.org/10.1371/journal.pone.0123843
23. Maisuria R, Norton A, Shao C, Bradley EW, Mansky K. Conditional loss of MEF2C expression in osteoclasts leads to a sex-specific osteopenic phenotype. *Int J Mol Sci*. 2023;24(16):12686. https://doi.org/10.3390/ijms241612686
24. Ha J, Choi HS, Lee Y, Kwon HJ, Song YW, Kim HH. CXC chemokine ligand 2 induced by receptor activator of NF-kappa B ligand enhances osteoclastogenesis. *J Immunol*. 2010;184(9):4717-4724. https://doi.org/10.4049/jimmunol.0902444
25. Takayanagi H, Kim S, Matsuo K, et al. RANKL maintains bone homeostasis through c-Fos-dependent induction of interferon-beta. *Nature*. 2002;416(6882):744-749.
26. Schneider WM, Chevillotte MD, Rice CM. Interferon-stimulated genes: a complex web of host defenses. *Annu Rev Immunol*. 2014;32(1):513-545. https://doi.org/10.1146/annurev-immunol-032713-120231
27. Du J, Liu Y, Wu X, et al. BRD9-mediated chromatin remodeling suppresses osteoclastogenesis through negative feedback mechanism. *Nat Commun*. 2023;14(1):1413.
28. Shi YJ, Matson C, Lan F, Iwase S, Baba T, Shi Y. Regulation of LSD1 histone demethylase activity by its associated factors. *Mol Cell*. 2005;19(6):857-864.
29. Roizman B. The checkpoints of viral gene expression in productive and latent infection: the role of the HDAC/CoREST/LSD1/REST repressor complex. *J Virol*. 2011;85(15):7474-7482. https://doi.org/10.1128/JVI.00180-11
30. Song Y, Dagil L, Fairall L, et al. Mechanism of crosstalk between the LSD1 demethylase and HDAC1 deacetylase in the CoREST complex. *Cell Rep*. 2020;30(8):2699-711 e8.
31. Zhao Q, Li S, Li N, et al. miR-34a targets HDAC1-regulated H3K9 acetylation on lipid accumulation induced by homocysteine in foam cells. *J Cell Biochem*. 2017;118(12):4617-4627. https://doi.org/10.1002/jcb.26126
32. Vecera J, Bartova E, Krejci J, et al. HDAC1 and HDAC3 underlie dynamic H3K9 acetylation during embryonic neurogenesis and in schizophrenia-like animals. *J Cell Physiol*. 2018;233(1):530-548. https://doi.org/10.1002/jcp.25914
33. Astleford K, Campbell E, Norton A, Mansky KC. Epigenetic regulators involved in osteoclast differentiation. *Int J Mol Sci*. 2020;21(19):7080. https://doi.org/10.3390/ijms21197080
34. Cao C, Vasilatos SN, Bhargava R, et al. Functional interaction of histone deacetylase 5 (HDAC5) and lysine-specific demethylase 1 (LSD1) promotes breast cancer progression. *Oncogene*. 2017;36(1):133-145.
35. Bennesch MA, Segala G, Wider D, Picard D. LSD1 engages a corepressor complex for the activation of the estrogen receptor alpha by estrogen and cAMP. *Nucleic Acids Res*. 2016;44(18):8655-8670.
36. Nakamura T, Imai Y, Matsumoto T, et al. Estrogen prevents bone loss via estrogen receptor alpha and induction of Fas ligand in osteoclasts. *Cell*. 2007;130(5):811-823.
37. Martin-Millan M, Almeida M, Ambrogini E, et al. The estrogen receptor-alpha in osteoclasts mediates the protective effects of estrogens on cancellous but not cortical bone. *Mol Endocrinol*. 2010;24(2):323-334. https://doi.org/10.1210/me.2009-0354
38. Kim HN, Ponte F, Nookaew I, et al. Estrogens decrease osteoclast number by attenuating mitochondria oxidative phosphorylation and ATP production in early osteoclast precursors. *Sci Rep*. 2020;10(1):11933. https://doi.org/10.1038/s41598-020-68890-7
39. Indo Y, Takeshita S, Ishii KA, et al. Metabolic regulation of osteoclast differentiation and function. *J Bone Miner Res*. 2013;28(11):2392-2399. https://doi.org/10.1002/jbmr.1976
40. Zeng R, Faccio R, Novack DV. Alternative NF-kappaB regulates RANKL-induced osteoclast differentiation and mitochondrial biogenesis via independent mechanisms. *J Bone Miner Res*. 2015;30(12):2287-2299. https://doi.org/10.1002/jbmr.2584
41. Nishikawa K, Iwamoto Y, Kobayashi Y, et al. DNA methyltransferase 3a regulates osteoclast differentiation by coupling to an S-adenosylmethionine-producing metabolic pathway. *Nat Med*. 2015;21(3):281-287. https://doi.org/10.1038/nm.3774
42. Jin Z, Wei W, Yang M, Du Y, Wan Y. Mitochondrial complex I activity suppresses inflammation and enhances bone resorption by shifting macrophage-osteoclast polarization. *Cell Metab*. 2014;20(3):483-498. https://doi.org/10.1016/j.cmet.2014.07.011
43. Bae S, Lee MJ, Mun SH, et al. MYC-dependent oxidative metabolism regulates osteoclastogenesis via nuclear receptor ERRalpha. *J Clin Invest*. 2017;127(7):2555-2568.
44. Gaber T, Strehl C, Buttgereit F. Metabolic regulation of inflammation. *Nat Rev Rheumatol*. 2017;13(5):267-279. https://doi.org/10.1038/nrrheum.2017.37

45. Syberg S, Petersen S, Beck Jensen JE, et al. Genetic background strongly influences the bone phenotype of P2X7 receptor knockout mice. *J Osteoporos*. 2012;2012:391097-391099. https://doi.org/10.1155/2012/391097
46. Chapp AD, Nwakama CA, Thomas MJ, Meisel RL, Mermelstein PG, Mermelstein PG. Sex differences in cocaine sensitization vary by mouse strain. *Neuroendocrinology*. 2023;113(11):1167-1176. https://doi.org/10.1159/000530591
47. Zanotti S, Kalajzic I, Aguila HL, Canalis E. Sex and genetic factors determine osteoblastic differentiation potential of murine bone marrow stromal cells. *PLoS One*. 2014;9(1):e86757. https://doi.org/10.1371/journal.pone.0086757
48. Nalawansha DA, Pflum MK. LSD1 substrate binding and gene expression are affected by HDAC1-mediated deacetylation. *ACS Chem Biol*. 2017;12(1):254-264.
49. Cantley MD, Fairlie DP, Bartold PM, Marino V, Gupta PK, Haynes DR. Inhibiting histone deacetylase 1 suppresses both inflammation and bone loss in arthritis. *Rheumatology (Oxford)*. 2015;54(9):1713-1723. https://doi.org/10.1093/rheumatology/kev022
50. Algate K, Haynes D, Fitzsimmons T, et al. Histone deacetylases 1 and 2 inhibition suppresses cytokine production and osteoclast bone resorption in vitro. *J Cell Biochem*. 2020;121(1):244-258. https://doi.org/10.1002/jcb.29137

© The Author(s) 2024. Published by Oxford University Press on behalf of the American Society for Bone and Mineral Research. This is an Open Access article distributed under the terms of the Creative Commons Attribution Non-Commercial License (https://creativecommons.org/licenses/by-nc/4.0/), which permits non-commercial re-use, distribution, and reproduction in any medium, provided the original work is properly cited. For commercial re-use, please contact journals.permissions@oup.com
JBMR Plus, 2025, 9, ziae142
https://doi.org/10.1093/jbmrpl/ziae142
Research Article